# Fatigue life estimation of riveted joints using crack growth concept

**†*Jakub Šedek[1], Tomáš Mrňa[1], Ivan Mlch[1], Pavel Kucharský[1]**

[1]Department of Strength of Structures, Czech Aerospace Research Centre, Beranových 130, 19905 Prague – Letňany, Czech Republic.

*Presenting author: sedek@vzlu.cz
†Corresponding author: sedek@vzlu.cz

## Abstract

Fatigue life estimation of riveted joints with countersunk head was performed by the crack growth analysis and results were compared with the experimental observation. The multi-site damage (MSD) in the skin made from the aluminium alloy D16č ATV was assumed so that the simultaneous development of fatigue cracks emanating from holes in the same structural element was studied. The equivalent initial flaw size approach (EIFS) was employed. The series of ten simultaneously growing cracks was analysed by methods of linear elastic fracture mechanic and crack growth concept utilizing FASTRAN model. Stress intensity factors used in the crack growth law were determined from the finite element model created in ABAQUS FE package. Cracks development under loading at several load levels was simulated. Assuming initial corner cracks of 0.125 mm in size, the analysis results show the fatigue lives close to the experimentally determined S-N curve of tested specimens. The considerable part of the fatigue life of the joint can be attributed to the crack growth. The analysis results exhibit that the smaller load level yields the longer crack initiation. The simulated fatigue life of tested specimens determined by the crack growth concept can be used as the upper bound for the design purposes in involved joint configuration very well.

**Keywords:** Crack, Fatigue, FEM, MSD, Rivets

## Introduction

The connection of skins in an airplane structure is commonly made by rivets. Several types including solid rivets and blind rivets with round, flat, countersunk or pan head are being used. The countersunk head is special for its smooth surface of final outer side and for that it is used in aerospace widely. The disadvantage is the sharp shape in the hole caused by the countersunk and due to this fact, the fatigue life can be reduced considerably in comparison with rivets that require blind hole [1]. Expected stress peak on the hole edge does not need to be crucial because it can be reduced by residual stresses created during riveting process [2][3][4]. The residual stress can beneficial to the fatigue performance of riveted joints [5].

The durability of the joint is influenced by many factors and the fatigue life prediction is far from easy. The experimental evaluation is used for S-N curve determination which depicts cyclic stress amplitude versus number of cycles to failure. The fatigue life under constant amplitude loading at different load level can be predicted based on the S-N curve. Alternatively, more complex prediction models can be employed [6][7]. The means of fracture mechanics are also utilized [8][9]. The fatigue life of the joint is analysed according to a crack advance, but some initial crack should be assumed. The analysis can be conducted for different joint configurations without experimental S-N curve data, but the crack growth

rate data together with crack growth model are necessary. The introduced analysis is performed by this approach and the comparison with the experimental S-N curve is finally presented.

## Experimental evaluation of fatigue life

In test laboratories of the Czech Aerospace Research Centre, the experimental fatigue life verification of several rivet types was carried out [1]. The result of countersunked rivets were different from other types due to the failure occurring in the centre part representing a skin, while the failure of straps was common in other rivet types (see Figure 1). The quadriplicated configuration of the test specimen was used. The methodology of fatigue tests was based on fatigue loading until failure. Whereas, after the failure of one joint, the specimen was split up to enable further testing of remaining joints of the specimen. The joint consisted of the central part 1.5 mm thick and two 0.8 mm thick strips symmetrically placed on the top and the bottom. The rivets in each joint were arranged in four rows with five rivets. The rivets were specified as 5DuZz 3x7P according to the manufacturer standards. The main head of the rivet is countersunked, the shank is 3 mm in diameter and the secondary head is being created by squeezing the rivet shank with final cylindrical shape. The type of rivets was the same in all joints in the test specimen. A set for the fatigue life evaluation consisted of six pieces of test specimens.

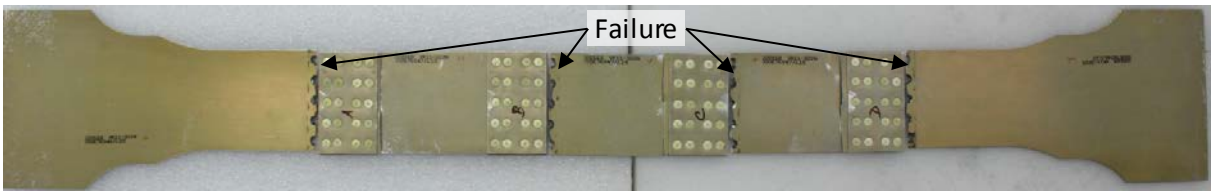


**Figure 1: Tested and analysed fatigue lives of the riveted joints with countersunk head.**

Specimens were loaded by monotone loading with constant amplitude of the force, the stress ratio $R$ = 0.05 and the frequency from 3 Hz up to 8 Hz. The tests were performed at room temperature and ambient laboratory conditions. The uniaxial hydraulic test machines INOVA ZUZ 100 with load cell capacity of 100 kN was used for fatigue tests. The maximum stress values $\sigma_{max}$ of the central part gross section were defined on five levels from 83 MPa up to 152 MPa to cover S-N curve uniformly.

During the fatigue experiment the failure of the central part only has been occurring. No failure of the rivets happened. Unfortunately, due to the cover by straps, the crack growth was not able to monitor. The cracks developed through rivet holes and only the final failure was noticed. The life of the joints was in the range of 1e4 up to 2e6 cycles. The fatigue data were evaluated using the linear regression by means of a linear model represented by the equation

$$\log N_f = A_1 + A_2 \log \sigma_{\max} \tag{1}$$

with determined coefficients for tested configuration $A_1$=12.87 and $A_2$=3.98 and coefficient of determination $r^2$ = 0.98.

After the failure the crack surface was photographically documented. The example tested under load conditions with $\sigma_{max}$ = 48.1 MPa is shown in Figure 2. Based on the fractographic examination carried out on a macro scale utilising optical microscopy the crack initiation

points were identified. In the Figure 2 they are marked by red arrows. Fatigue cracks initiated in the rivet holes. The crack initiation was clear at site holes shown in Figure 3. In the detail the corner crack shape is obvious and the surrounding crack surface structure shows changes in the macromorphology of the surface. The finding indicates the damage of the surrounding area in the cross section due to the final failure.

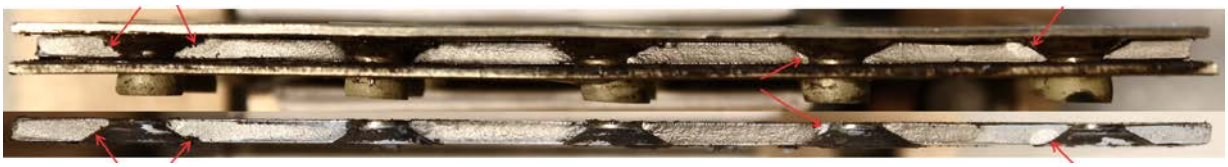

**Figure 2: Several crack initiations from the rivet holes; $\sigma_{max}$ = 48.1 MPa.**

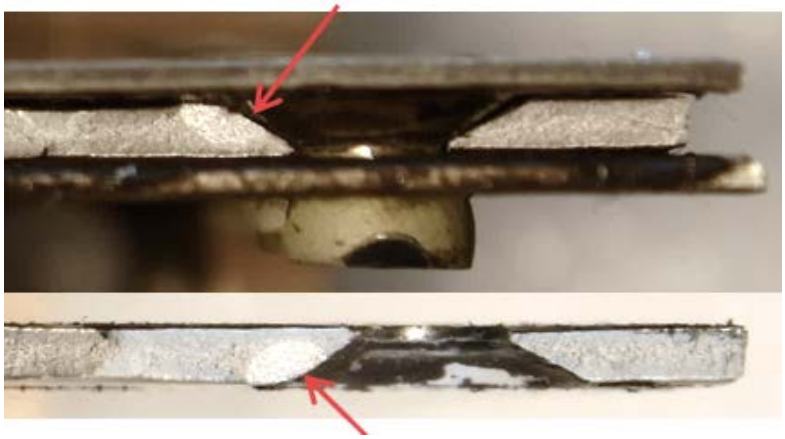

**Figure 3: Detail of crack initiation point at the side hole; $\sigma_{max}$ = 48.1 MPa.**

The interesting note is that the crack initiation spots were located mainly at the corner of intersection of the countersunk and the outer surface and not at the opposite sharp edge as can be expected due to stress concentration effect.

### Simulation of the fatigue life

The joints life can be split into the period of a crack initiation and a crack growth. The boundary between these periods is not strict and is very difficult to distinguish it quantitatively. In microscale the transition depends on the microcrack size and the microstructural barriers. The size of the crack at the transition point can be different for different types of materials. The point of the transition may be specified rather qualitatively. The initiation period is the surface phenomenon and the crack growth period starts if the crack growth resistance of the material is controlled by the crack growth rate [8]. The initiation period can be significant portion of the life. However in the airplane structures the crack growth period is being essential and the considerable attention is paid to it.

The macromorphology of inspected failure surfaces of tested specimens indicated several cracks emanating from the rivet holes. The cracks growth was not documented due to the straps that covered the cracks for the hole life of the joints. The simulation of crack growth could point out the severity of the period of crack growth in the fatigue life.

A simultaneous crack growth scenario was chosen to analyse employing equivalent initial flaw size (EIFS) approach. According to Joint Service Specification Guide of USAF for

aircraft structures (JSSG-2006) [9] small imperfections equivalent to an 0.127 mm radius corner flaw resulting from material and structure manufacturing and processing operations are assumed to exist in each hole of each element in the structure. In slow crack growth structure at holes and cut-outs, the assumed initial flaw is a 1.27 mm radius corner flaw at one side of the hole. When the primary damage and crack growth originates in a fastener hole and terminates prior to member or element failure, continuing damage should be an 0.127 mm radius corner flaw plus the amount of growth which occurs prior to primary element failure emanating from the diametrically opposite side of the fastener hole at which the initial flaw was assumed to exist. The presumption of initial 1.27 mm flaw can be sometimes conservative but it is prescribed to declare the crack resistant feature of the structure.

In the presented cracks scenario the cracks were developing simultaneously from the same size in configuration of corner cracks of 0.13 mm in size located at the edge of countersunked holes. This arrangement was chosen in order not to give priority to a one larger crack. The analysis of crack growth was performed by step-by-step routine so that the cracks were extended from the previous configuration based on the computed crack increment. The characteristics of linear elastic fracture mechanics for each modeled step were determined from finite element model and the crack extension between modeled steps was determined by the crack growth model.

**Numerical model**

The numerical model of cracks configuration in each step was created in the FE package ABAQUS 2017. A symmetry was applied on the model so that only one quarter of the model was analysed. The example of crack configuration is shown in Figure 4. Model was discretized by tetrahedral (C3D4) and hexahedral elements (C3D8I). The mesh was refined around a crack front using only hexahedral elements stacked in ten layers (see Figure 5) with the smallest element dimension of about 0.002 mm. Regular mesh around a crack front is used to have a good results of contour integral for stress intensity factor calculation. Isotropic linear elastic material model with E = 72 000 MPa and ν = 0.33 was employed. The model was loaded by stress applied on tension site and boundary conditions respected the used symmetry.

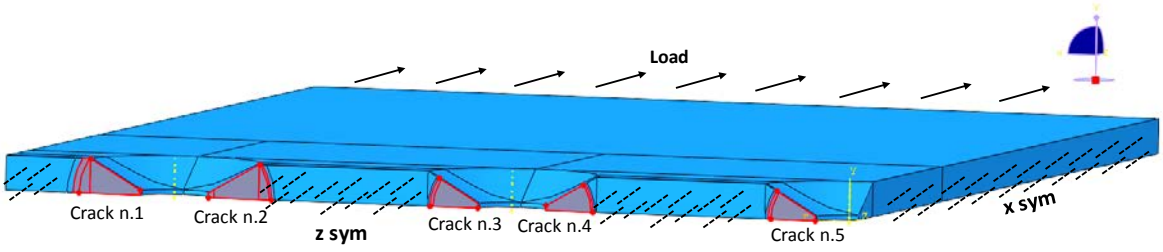


**Figure 4: 1/4 model of the skin part including cracks; top-front view on the geometry.**

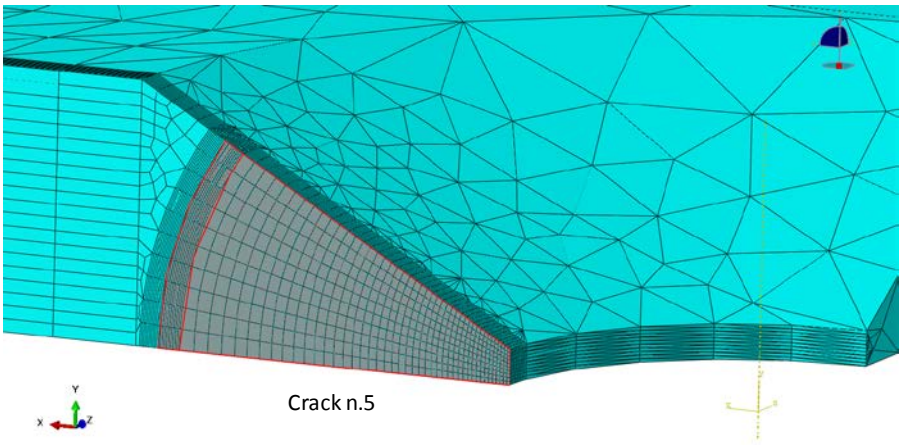


**Figure 4: Detail of the mesh around the crack n. 5.**

The stress intensity factor $K_I$ was determined by internal ABAQUS routine using contour integral method. Only the opening mode I was assumed in fracture mechanics parameters determination thus the $K$ always corresponds to mode I if stated without index in this work. There were from ten up to twenty contours evaluated in ten layers around a crack front typically. The mean value of the stress intensity factor from each contour was determined and one mean value $K_{char}$ from all layers was used as characteristic for a crack. Typical normalized stress intensity factors $K/K_{char}$ according to contours are plotted in Figure 5. The value of $K$ stabilizes after some contours away from the crack front except the one on the side of the crack (the blue dots in Figure. 5). The mean value eliminates this discrepancy.

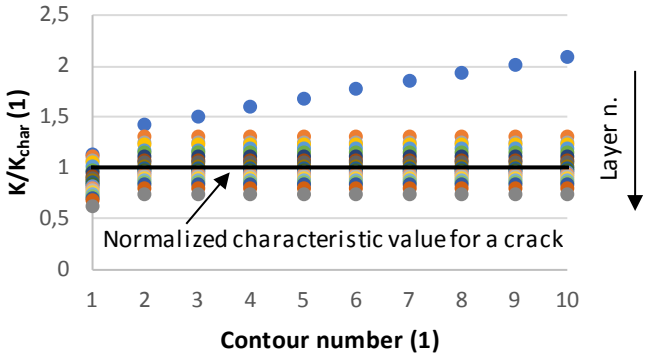


**Figure 5: Stress intensity factor around the crack front of the crack n.5 with the length of 2.1 mm.**

## Material data

In the numerical model cracks were extended at the same moment of elapsed cycles. The crack increments were determined by the crack growth model FASTRAN. The specimens were loaded with constant amplitude and despite the basic Paris law could be sufficient, more sophisticated model was used. At high crack growth rates, the effect of constrained loss can be expected, but only some models can capture this effect.

The crack growth rate data were used according to [11], where the data of Russian alloy D16CzATWH are documented. The crack growth properties are considered to be similar to the 2024-T3 alloy [12]. These data were used in presented work based on the results from

preliminary data testing. The results of simulated crack growth under constant amplitude loading in M(T) specimens using D16czATWH data for FASTRAN model were close to experimentally observed growth in specimens made from D16cATV. The crack growth rate data were interpolated by linear relationship in the form

$$\frac{\Delta a}{\Delta N} = C\left(\Delta K_{eff}\right)^{m} \tag{2}$$

with coefficient $C$ = 1.2e-10 and $m$ = 3.5. The effective value of stress intensity factor $K_{eff}$ depends on the opening stress intensity factor $K_{open}$ according to

$$\Delta K_{eff} = K_{\max} - K_{open} \tag{3}$$

$K_{open}$ is determined by the FASTRAN model considering load history by semi-analytical method. It requires the value of constraint factor α. The implementation in AFGROW [13] enables using one constraint value through the whole crack growth or two values according to crack growth rates at transitions points from plane strain to plane stress. These rates are attributed to points of flat-to-slant transition visible on fracture surfaces [8, 14]. The rate of 1e-7 m/cycle together with α = 2 were used for plane strain transition point and the rate of 2.5e-6 together with α = 1.2 were used for plane stress transition point.

The cracks were characterised by the shape function $\beta$. Its values were determined in step points normalizing the values of stress intensity factor $K_{FEM}$ determined from the numerical model by the term $\sigma\sqrt{\pi a}$, where $\sigma$ denotes the remote stress and $a$ is the crack length.

$$\beta = \frac{K_{FEM}}{\sigma\sqrt{\pi a}} \tag{4}$$

The crack increments to find the crack fronts in the step $i+1$ were determined from the actual step $i$ extrapolating the $\beta$ values linearly from previous points $i-1$ and actual point $i$. The resulting values of $\beta$ therefore occur in zig-zag pattern around middle theoretical curve. In order to avoid this behaviour, the iteration process should be employed as presented in [15], but it was not used in this work accepting some loss of accuracy.

## Cracks growth

The analysis of crack growth was carried out step-by step. The multi-side damage (MSD) scenario was assumed and all cracks were influencing each other through the simulation during the whole fatigue life. This type of analysis is not common due to its cost. More convenient is to analyse crack extension of the most loaded crack and after reaching the opposite side in the load carrying cross-section, the crack increment of the other crack is determined. Note that the crack increment during the growth of primary crack must be included. The initial crack length for all cracks was 0.13 mm assuming the crack shape as a circle section. A crack was therefore corner shaped up to reaching the whole thickness.

## Results

The analysis of fatigue life was performed with the $\sigma_{\max}$ = 48, 83 and 112 MPa independently. At each step of crack increments the numerical model was adapted in order to obtain the values of shape function. The shape function plots are in Figure 6.

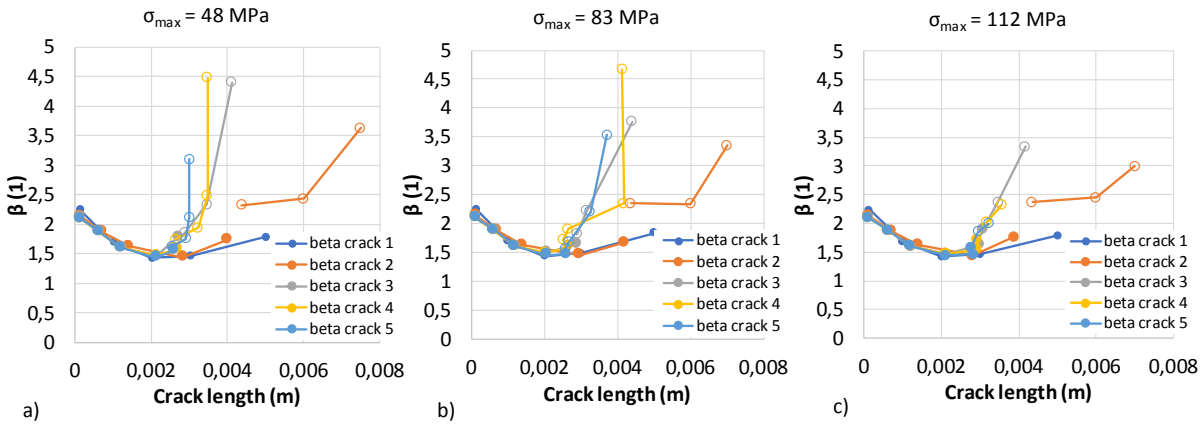


**Figure 6: Shape functions of cracks in analyses with a) σmax = 48 MPa b) σmax = 83 MPa c) σmax = 112 MPa.**

The shape function for small crack lengths is identical up to the size of 2 mm that corresponds to the change of the shape from the corner crack to the through crack. Up to this point cracks do not influence each other. The other change of the shape function occurs when the crack terminates. The full dots mark the state before terminating of the crack n. 1 and the circle dots correspond to the crack after that. The rapid rise of $\beta$ value for the crack n. 2 immediately after terminating the crack n. 1 is obvious.

From the plot of crack growth curves shown in Figure 7, it is clear that the fatigue life is determined by the crack n. 1. After terminating the crack n. 1 the other cracks growth is very fast.

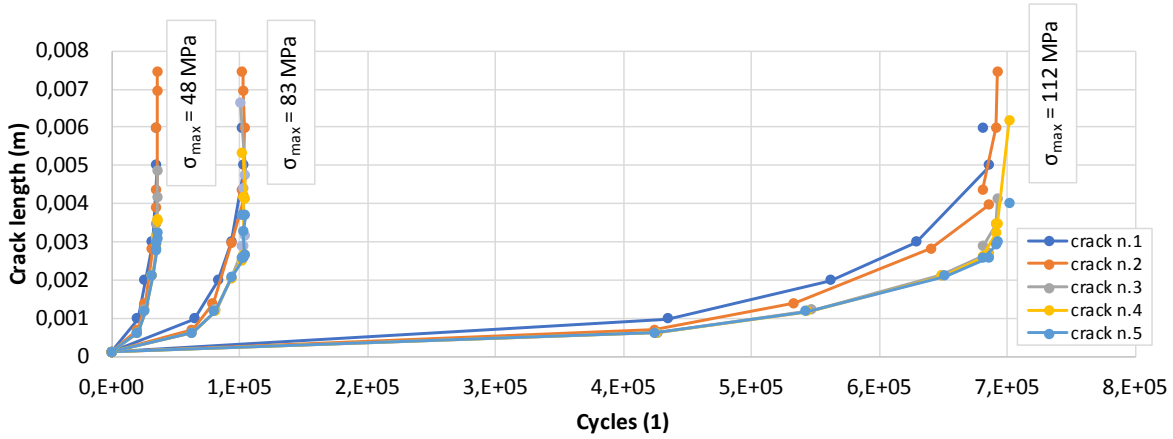


**Figure 7: Shape functions of cracks in analyses with σmax = 48, 83 and 112 MPa.**

Based on the result that the fatigue life is mainly determined by the crack n.1 the fatigue life with the levels $\sigma_{max}$ = 64 MPa and 152 MPa was determined using the shape function of the crack n. 1. The results are shown in logarithmical plot in Figure 8 together with the experimental results of specimen lives. The test data can be interpolated by power function drawn in log-log plot by linear curve.

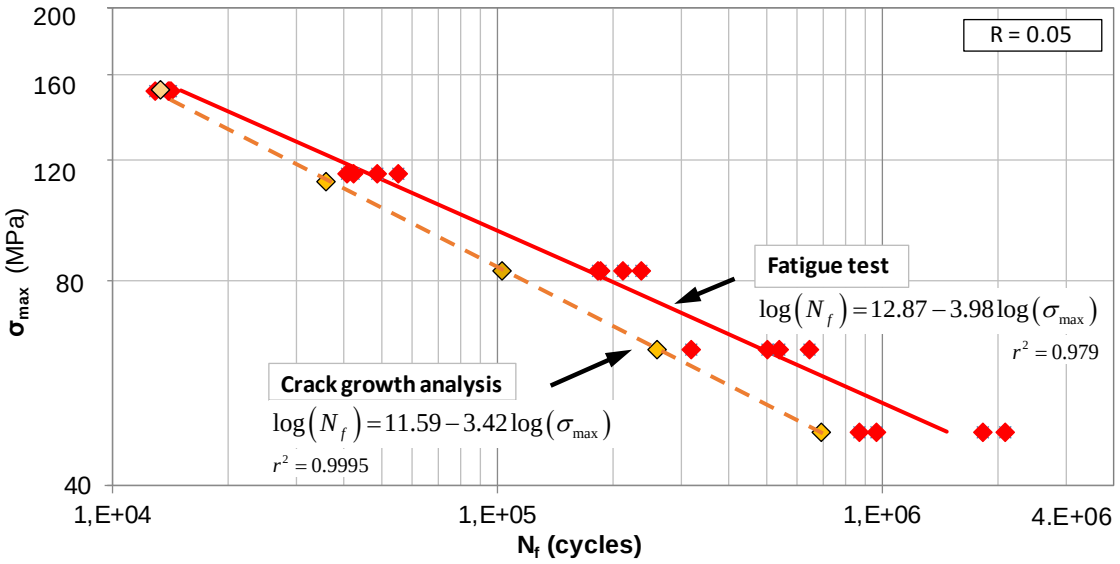


**Figure 8: Fatigue life of joint specimens; crack growth analysis and test data.**

## Discussion and conclusion

The fatigue life of the specimens representing riveted joint of airplane skin made from aluminium alloy was analysed. The experimental evaluation of the life was performed on several load levels under load cycle asymmetry $R = 0.05$. In logarithmical axes plot the test data can be interpolated by linear regression curve.

The analysis of fatigue live was also performed by means of linear elastic fracture mechanics and crack growth model. The multi-site damage (MSD) was assumed so that the numerical model of the part representing the skin was created and the shape function for each crack was determined. The analysis of fatigue life was carried out using equivalent initial flaw size approach (EIFS). The simultaneous crack growth was assumed. Provided initial corner cracks of 0.125 mm in size, the analysis results show the fatigue lives close to the experimentally determined S-N curve of tested specimens. The considerable part of the fatigue life of the joint can be therefore attributed to the crack growth. The analysis results exhibit the smaller load level yields the longer crack initiation and also the higher scatter of the fatigue life.

The crack initiation process is the surface phenomenon and can be covered computationally very hardly without relevant material data [8]. The presented analysis shows that in involved joint configuration the simulated fatigue life determined by the crack growth concept can be used as the upper bound for the design purposes successfully.

## Acknowledgement

This work was funded by the Ministry of Industry and Trade of the Czech Republic in the framework of the Institutional Support of Research Organizations.

### References

[1] T. Mrňa et al. (2018) The fatigue strength of various mechanical double shear rivet joints of D16čA TV sheets, Lufinka A. et al., (eds.). *Experimental Stress Analysis 2018*, Book of extended abstracts, June 5th – 7th, 2018, Harrachov, Czech Republic: Czech Society for Mechanics, 286-291, ISBN 978-80-270-4061-2.

[2] Wronicz, W. and Kaniowski, J. (2014) The analysis of the influence of riveting parameters specified in selected riveting instructions on residual stresses, *Fatigue of Aircraft Structures* **1** 63- 71, doi: 10.1515/fas-2014-0005.
[3] Zheng, B., Yu, H., Lai, X. and Lin, Z. (2016) Analysis of Residual Stresses Induced by Riveting Process and Fatigue Life Prediction *Journal of Aircraft* **53**, No. 5, DOI: 10.2514/1.C033715
[4] Szymczyk, L. and Godzimirski, J. (2012) The influence of riveting process on sheets fatigue life - The stress state analysis, *Acta Mechanica et Automatica* **6** (1), 74-81.
[5] Ransa, C.D., Alderliestena, R.C. and Straznicky, P.V. (2009) Assessing the effects of riveting induced residual stresses on fatigue crack behaviour in lap joints by means of fractography, *International Journal of Fatigue* **31** (2), 300-308.
[6] Skorupa, M. et al. (2017) Fatigue life predictions for riveted lap joints, *International Journal of Fatigue* **94,** 41–57. doi: 10.1016/j.ijfatigue.2016.09.007.
[7] Skorupa, M. et al. (2015) Fatigue life prediction model for riveted lap joints, *Engineering Failure Analysis* **53,** 11-123.
[8] Schijve, J. (2010) Fatigue of structure and materials, 2nd edition, *Springer*, 621 pages, ISBN-13: 987-1-4020-6807-2.
[9] JSSG-2006 (1998) Joint service Specification Guide: Aircraft Structures, *Department of Defense of USA*, 148 pages.
[10] Zamani P. et al. (2015) Numerical Investigation on Optimizing Fatigue Life in a Lap Joint Structure, World Academy of Science, *Engineering and Technology International Journal of Civil and Environmental Engineering* **9** (5), 647-653.
[11] Ziegler, B. et al. (2011) Application of a strip-yield model to predict crack growth under variable-amplitude and spectrum loading – Part 2: Middle-crack-tension specimens, *Engineering Fracture Mechanics* **78**, 2609–2619.
[12] Schijve J. et al. (2004) Fatigue crack growth in the aluminum alloy D16 under constant and variable amplitude loading. *International Journal of Fatigue* **26**, 1–15.
[13] Harter, J. A. (2008) AFGROW users guide and technical manual, *Air Force Research Laboratory*, AFRL-VA-WP-TR-2008-XXXX.
[14] Běhal J and Nováková L. (2013) Stress state factor evaluation based on a fractographic analysis for use in the crack growth FASTRAN retardation model of the AFGROW computing code, *Engineering Failure Analysis* **35**, 645–651.
[15] Šedek, J., Běhal, J. and Siegl, J. (2015) Structure overloading evaluation based on the identification of subcritical crack increments, *Engineering Failure Analysis* **56**, 265-274.